Indian Journal of Chemical Technology
Vol. 25, March 2018, pp. 208-215

Performance of WO_3 nanoparticles in photocatalytic conversion of greenhouse gases under visible light irradiation

Maryam Torabi Merajin[1], Mohammad Nasiri*[,1], Ebrahim Abedini[1]& Shahram Sharifnia[2]

[1]Department of Chemistry, Malek-ashtar University of Technology, Shahin-shahr 83145/115, Iran

[2]Catalyst Research Center, Chemical Engineering Department, Razi University, Kermanshah 67149-67246, Iran

E-mail: nasiri@mut-es.ac.ir

Received 9 January 2017; accepted 28 August 2017

The direct photoconversion of carbon dioxide and methane is investigated in an appropriate gas-phase batch reactor under visible light irradiation. WO_3 nanoparticles coated on stainless steel webnet have used as photocatalyst. WO_3 nanoparticles are synthesized and characterized by SEM, XRD, EDX, FTIR and UV-vis spectra analyses. SEM images indicate that WO_3 nanoparticles were well coated on the surface of the webnet. The XRD analysis confirm monoclinic structure and average particle size about 100 nm for the WO_3 nanoparticles. Also, the FTIR analysis exhibit the structure of tungsten oxide. The results of UV–vis show that the visible light absorbance spectrum of WO_3 are more efficient than TiO_2 and ZnO. The conversions of 28% and 13.3% for CO_2 and CH_4 has been found by WO_3 under visible light, respectively.

Keywords: Greenhouse gases, Carbon dioxide, Methane, Photocatalyst, WO_3 nanoparticles

According to the Intergovernmental Panel on Climate Change (IPCC, 2005), most of the global warming over the past 50 years is caused by human activities. Human influences on climate change are expected to be continuing to change the atmospheric composition throughout the 21st century. Greenhouse gases (GHGs) such as CO_2, CH_4, N_2O, HFCs, PFCs, and SF_6 are the primary causes of global warming. Carbon dioxide, which is mostly released from fossil fuel combustion, is known as the most important greenhouse gas and major responsible for increasing Earth's average surface temperature[1]. The global concentration of CO_2 in the atmosphere is increasing[1] and this accelerates the greenhouse effect. The Kyoto Protocol of 1997 on greenhouse gases (GHGs) emission has evidenced the necessity to control the emissions not only of CO_2, but also of CH_4 and N_2O, which respectively contributed 7 and 9% to the Global Warming Potential (GWP) (with reference to the CO_2 equivalent emissions, using GWP values for a100-year time horizon)[2].

Among anthropogenic greenhouse gases, methane and carbon dioxide have the greatest effects on the climate. High concentration and emission of these air pollutants are related to human, animal health and ecological damage. Therefore, efforts are made to find the effective and new methods to reduce or convert CO_2 and CH_4 into useful compounds[3]. Unfortunately, it is not easy to convert these stable molecules to other useful chemicals at mild reaction condition. Thus, alternative methods that can lower the reaction temperature are desired. It can be proposed that the use of photoenergy with photocatalyst would break the thermodynamic barrier of endothermic reactions to proceed at lower temperature[4].

Semiconductor catalysts have received considerable attention in recent years because of their photocatalytic activity for initiating redox reactions[5-7]. Conversion of CO_2 is a reduction reaction, while that of CH_4 is an oxygenation process. This photocatalytic process is an ideal redox reaction in which CO_2 and CH_4 are converted at the same time. There are some studies on the simultaneously conversion of CO_2 and CH_4 by photocatalytic process[3,4,7-15].

Now a days, the use of visible-light-responsive photocatalysts are more preferred, because of the future prospect of using sunlight and indoor light in practical applications[16]. The first process of photocatalysis is the excitation of the catalyst by absorption of photons with energy equal to or larger than the band gap energy of the semiconductor. Most of semiconductor catalysts have large band gaps, which are match to the UV light, only 4% of the sunlight spectrum[17]. In recent years, many efforts have been focused on the modification of TiO_2 and development of novel photocatalytic materials with appropriate band gaps. Among them, nanostructured WO_3 with a smaller band gap (~2.6 eV) is being rapidly developed[18]. WO_3 semiconductor, having yellow-green color, has been considered as a photocatalyst operating under visible light irradiation[19]. Tungsten oxide (WO_3) is a visible light-responsive photocatalyst that absorbs light up to 480 nm. Compared with the mixed metal oxides and doped oxides, WO_3 is easy to prepare, modify and used to coat substrates. WO_3 also

is harmless and is stable in acidic and oxidative conditions[20]. Functional nanostructured WO_3 materials with interesting optical, electrical, chemical and catalytic properties could be used in a wide range of practical applications: electrochromic smart windows, gas sensors, photovoltaic devices, lithium-ion batteries, hydrogen generation, electrocatalysts and photocatalysts. The different and attractive WO_3 nanostructures have been fabricated by ultrasonic spray pyrolysis, hydrothermal treatment, sol-gel, thermal evaporation, cathodic deposition, electrophoretic deposition and electro-chemical anodization techniques[21].

The photocatalytic conversion of CO_2 by WO_3 has been studied in only a few reports[22-24]. Also, prior studies reported the use of WO_3 for CH_4 photoconversion[25-32]. However, up to now any papers have not been reported on the concurrently photocatalytic conversion of CO_2 and CH_4 by WO_3 under visible light. In this study, WO_3 nanoparticles were synthesized by a very simple and inexpensive method and coated on stainless steel webnet for visible light photocatalytic conversion of carbon dioxide in the presence of methane as the reductant under the mild conditions. The stainless steel webnet was selected as support because of the following reasons: the webnet structure provides a large surface area for WO_3 film; it is appropriate for gases passing through ventilation; the light can pass easily through the webnet pores; and it is resistance to various corrosions[11,12]. The experiments were done in an appropriate gas-phase self-designed batch reactor equipped with a temperature and pressure controller system. Also, the morphology, crystal structure, optical absorption and chemical composition of the prepared photocatalysts were characterized by scanning electron microscope (SEM), X-ray diffraction *(*XRD), Ultraviolet–visible (UV–vis), Energy-dispersive X-ray (EDX) and Fourier transform infrared (FTIR) analyses. To evaluate the relative photocatalytic activities of the obtained WO_3 nanoparticles, experiments were performed to compare their activities with those of commercial TiO_2 and ZnO under visible-light irradiation.

Experimental Section

Materials

$Na_2WO_4.2H_2O$ (99%), Ethanol (96%), nitric acid (65%), hydrochloric acid (37%) and acetone were obtained from Merck. All of the chemicals are of analytically grade purity and were used without further purification. The deionized water was used in catalyst preparation. Titanium dioxide P25 and ZnO (wurtzite hexagonal structure) were supplied by Degussa and Merck companies, respectively. The used CO_2, CH_4 and He gases were ultra-high pure (99.9%). Stainless steel webnet with mesh sizes of 120 as support was bought from Haidian Hardware Store of Beijing in China.

Preparation of WO_3 nanoparticles

WO_3 nanoparticles were prepared by direct precipitation. A solution of $Na_2WO_4.2H_2O$ (0.5 M) was obtained and heated at 80°C in a reflux. Hydrochloric acid (3.0 M) was added drop wise to the Na_2WO_4 solution until precipitation. The resulting product was centrifuged and washed for several times with deionized water to reach neutral solution *p*H. At this time, WO_3 nanoparticles settled in the bottom of centrifugal tube. After centrifuging, WO_3 nanoparticles were subjected to slow evaporation to remove the excess solvent at room temperature and then annealed in air at 400°C for 4 h[33,34].

Preparation of photocatalysts coated webnets

Immobilization of WO_3 nanoparticles on stainless steel webnets was done using a simple and efficient method which is ideal for industrial applications. This technique was originally developed by scientists at Netherlands Energy Research Foundation (ECN) for deposition of TiO_2 on quartz slides to prepare solar cells[35]. The same technique was applied with minor changes for preparing coatings of TiO_2 and ZnO on stainless steel webnets to use them as photocatalysts[13].

In order to coat support with titanium dioxide, first 2.5 g (±0.001 g) TiO_2 powder was added to 15 mL (±0.01 mL) ethanol as the base medium of the slurry. Ethanol was selected as solvent due to good dispersion of TiO_2, ZnO and WO_3 in a cloud-shape manner. Then, 5 mL of dilute nitric acid with a *p*H of 3.5 (±0.01) was added to the slurry to supply a suitable acidity in the slurry. As the acid is added, the slurry becomes more uniform and its cloudiness starts to disappear. To coat supports with ZnO and WO_3, the same above mentioned method was applied with difference in amount of precursor. 1.7 g (±0.001 g) of zinc oxide was added to 20 mL ethanol and, at the second step, 7 mL (+0.01 mL) of dilute nitric acid with a *p*H of 3.5 (±0.01) was added to the slurry. In order to coat support with WO_3, 1.0 g (±0.001 g) of Tungsten oxide was added to 25 mL ethanol and, at the second step, 10 mL (+0.01 mL) of dilute nitric acid with a *p*H of 3.5 (±0.01) was added to the slurry. These differences in the amounts of WO_3, TiO_2 and ZnO are due to the differences in their density, which follow such an

order: WO_3> ZnO >TiO_2. In all prepared catalyst, 0.4 g (±0.001 g) particles were coated on the surface of 415 cm^2 (±0.1 cm^2) mesh network.

The prepared slurry was sonicated for 30 min for suitable dispersion of powders and obtaining more uniform slurry. Next, stainless steel webnet was immersed into the slurry. The webnet was previously formed in cylindrical shape and cleaned with hydrochloric acid, acetone and distilled water to remove any organic and inorganic material attached to or adsorbed on the surface and dried under atmospheric conditions. Contact time for slurry adsorption by stainless steel webnet was 1 min. Then, the webnet was put into an oven for 12 h at 120°C (±1.0°C) for drying. In the final stage of coating process, the webnet was annealed at 350°C (±1.0°C) for 30 min.

Photocatalysts characterization methods

X-ray diffraction method using CuKα radiation has been used to study the structure of the synthesized nanoparticles. This study was carried out at room temperature by employing a Panalytical X'PertPRO (Holland) Advance X-ray differactometer with CuKα (λ=1.54°A) radiation using a tube voltage and current of 40 kv and 30 mA respectively. The sample was scanned from 10°-80° in 2θ with step size of 0.02° 2θ. The average crystallite size was calculated based on the XRD patters using the Sherrer's equation. The morphologies of the films at room temperature were characterized by a field emission scanning electron microscope (FESEM, TESCAN Company) equipped with an energy dispersive X-ray spectroscopy (EDX) attachment. The coated webnet samples were coated with a thin layer of gold before scanning for producing electric conductivity and viewed with the microscope at 30 kV. The elemental analysis of the synthesized WO_3 nanoparticles was performed by EDX Analysis. Fourier transform infrared (FTIR) spectra were recorded at room temperature on a Nicolet's Magna- IR System 550 FT-IR spectrometer with the samples pressed with KBr pellet from 4000 to 400 cm^{-1}. Diffuse-reflectance UV-vis spectra of the photocatalysts were recorded in the range 190–900 nm at room temperature using a Jasco V-670 spectrophotometer (Japan).

Photocatalytic reaction tests

In order to assess the photocatalytic efficiency of the prepared catalysts, photoreduction of the CO_2 and CH_4 gases under Visible illumination was investigated in a self-designed photocatalytic reactor. The details of the reactor have been reported elsewhere[11,12]. Figure 1 presents photographs of the actual photoreactor system and the coated WO3 over the webnet.

Fig. 1 — The present of (a) coated and uncoated cylindrical stainless steel webnets with WO_3 particles (b) open photocatalytic reactor with its cap and lamp situation and (c) the assemble photoreactor.

The photoreactor, comprised of coated particles over the stainless steel webnet, was assembled to transmit and spread light uniformly. The cap of mesh photoreactor was scaled using O-rings and checked if there was leakage. At the next step, the reactor was vacuumed and then it was filled in by gaseous feed (CO_2, CH_4 and He) to 60 psig of absolute total pressure. Total inner volume of reactor was 1.0 L (±0.01 L). Before starting the reaction, the gas feed concentration was analyzed through using on-line GC (equipped with a TCD detector), and then it was illuminated by UV lamp for 5 h continuously. After that, reactor continuously illuminated by a 125 W high pressure mercury lamp for 5 h. Each experiment was performed at about 60°C. A glass bulb with a special coating was used to filter out UV light. The doped quartz glass of the bulb filters out most of the UV radiation throughout the whole radiation spectrum of the lamp. Thus, the mostly short wave of UV-C and UV-Brays were retained more, and the long wave UV-A radiation was reduced by half of them (Osrum GmbH, Germany). In this study, the reactor volume and UV power intensity were selected similar to some investigations in CO_2 photocatalytic reduction[11,36-39]. The photocatalytic activity was calculated on the basis of CO_2 and CH_4 conversions.

Results and Discussion

Crystal structure of WO_3 nanoparticles

Phase analysis was carried out to understand the crystallinity and phase purity of the synthesized WO_3 nanoparticles. Figure 2 represents the XRD patterns of the synthesized WO_3 nanoparticles. The XRD spectra confirm the crystallinity with apparently monoclinic structure of WO_3, which has been further confirmed from Raman spectroscopic data presented later. The diffraction peaks in XRD patterns of WO_3 nanoparticles are indexed to the monoclinic phase of WO_3 (JCPDS no. 05-0364, unit cell parameters: a=7.2850, b=7.5170, c=3.8350 Å, β=90.1500°; space group: P21/a)[40] and no characteristic peaks from other crystalline impurities were detected, which indicates its high purity.

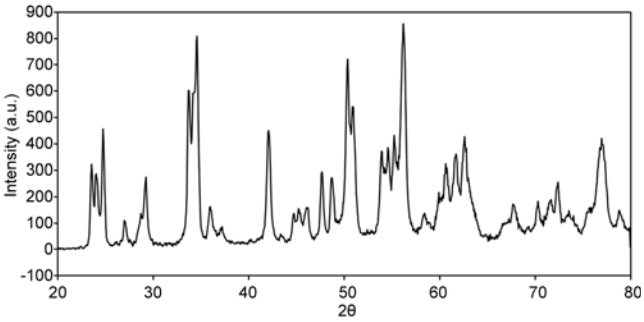

Fig. 2 — XRD spectra of the synthesized WO_3 nanoparticles.

The crystal size of WO_3 nanoparticles has been determined using the Scherrer's equation : $D = 0.9\lambda/B\cos\theta$; where D is the crystallite size (nm), λ is the wavelength of the X-ray radiation, θ is the Bragg's angle and B is the full width at half maximum (FWHM) of the peak at 2θ[41]. The average crystal size of synthesized WO_3 nanoparticles have been estimated as 100 nm.

Morphological properties of WO_3 nanoparticles

The FESEM examined the morphology and size of the samples (Fig. 3). The images were used to show how photocatalysts were coated on/in mesh network. The FESEM photograph of the WO_3 nanopartcles films on webnet shows well adherent surface morphology. As shown in Fig. 3(a), WO_3 coated on webnet were immobilized in a good state between woven fabrics of webnet and gases could easily pass through photocatalyst. The FESEM image of the WO_3/webnet photocatalyst suggests that a few numbers of cavities are dispersed on the surface of the photocatalyst (Fig. 3(b)). The cavities may be formed through the removal of organic matter in the paste during the annealing process. The highest magnification FESEM image of the WO_3/webnet photocatalyst is shown in Fig. 3(c), and it can be seen the uniform size of WO_3 nanoparticles on the support surface.

In order to find the chemical composition of the nanoparticles, EDX analysis was carried out. Fig. 3(d) shows the EDX analysis of the WO_3 nanoparticles. It was observed, just W and O elements without any remarkable impurity.

FTIR spectra of WO_3 nanoparticles

For further investigation of the surface property and to detect subtle phase information of the WO_3 nanoparticles, FTIR analysis was conducted. The FTIR spectrum of the WO_3 in the range of 400-4000 cm^{-1} is shown in Fig. 4. The FTIR spectrum confirms the formation of monoclinic WO_3 nanoparticles, showing the two strongest peaks at 761 and 815 cm^{-1} assigned to the stretching vibration of tungsten atom with neighboring oxygen atoms [υ(O−W−O)][42].

UV–Vis spectroscopy of WO_3 nanoparticles

Fig. 5(a) displays UV–vis diffuse reflectance spectra of WO_3 nanoparticles. The WO_3 shows absorption edge at around 485 nm. The absorption spectrum was further analyzed by plotting $(\alpha h\upsilon)^2$ against $h\upsilon$ or energy, based on Eq. (1).

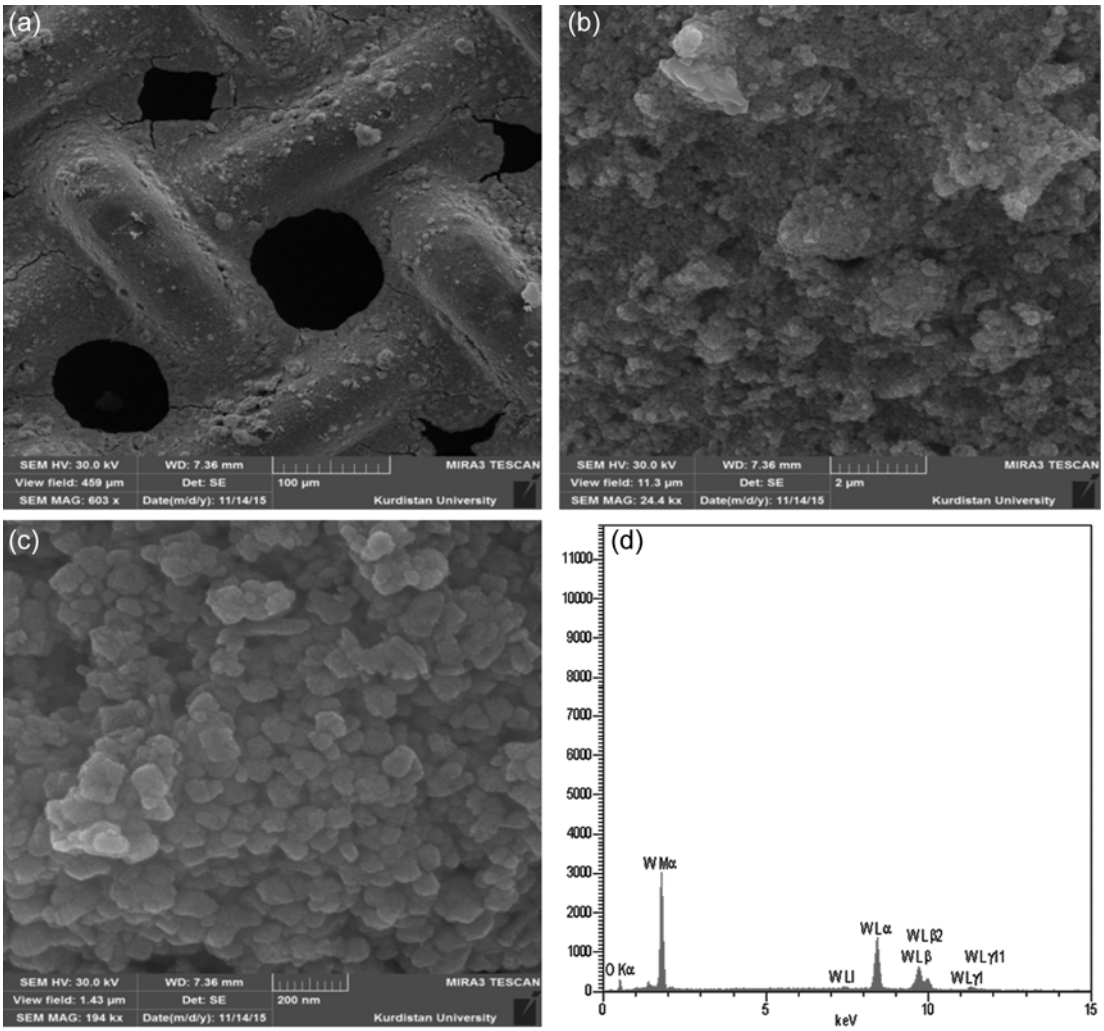

Fig. 3 — (a,b,c) FESEM images at different magnifications recorded onsynthesized WO_3 nanoparticles coated on webnet (d) EDX spectrum of WO_3 nanoparticles.

$$(\alpha h\upsilon)^2 = A(h\upsilon - Eg)^n (1)$$

where α is the absorption coefficient, A is a constant independent from frequency υ, n is the exponent that depends upon the quantum selection rules for the particular material, and Eg is the band gap of the material. This relationship gives the Eg by extrapolating the straight portion of $(\alpha h\upsilon)^2$ against $h\upsilon$ plot to the point α = 0 as shown in Fig. 5(b). Accordingly, synthesized WO_3 nanoparticles show band gap energy of approximately 2.77eV. This result has an agreement with other studies reporting a band gap energy for monocline crystalline WO_3 of approximately 2.8 eV[43]. It can be found that the synthesized WO_3 nanoparticles have great absorption at both ultraviolet and visible regions. This also means that these compounds have great photocatalytic activity under visible light irradiation. Because WO_3 has a relatively small band gap (2.6 eV to approximately 3.1 eV), it has photocatalytic activity at visible region[44].

Photocatalytic activity

The photocatalytic activity of WO_3/webnet catalysts was examined by measuring the conversion of CH_4 and CO_2 under visible light irradiation after 5 h experiment. Figure 6 shows the efficiency of synthesized WO_3 coated on webnet in photodegradation of CO_2 and CH_4 concurrently (an equal initial ratio of carbon dioxide and methane in the feed). The results indicated that there were obvious photocatalytic activities under visible-light irradiation for WO_3/webnet catalysts. Xin *et al*. have reported that the phase of WO_3 is the major influencing factor for photocatalytic activity, and the monoclinic phase has the highest photocatalytic reaction[45]. Monoclinic WO_3 is the most stable phase of

WO_3 and it possesses a low band gap energy (2.4-2.8 eV), which extends the light absorption to the visible region[46]. This fact makes it suitable catalyst for greenhouse gases treatment with solar energy. In this study, after 5 h irradiating, the conversion percentages of CH_4 and CO_2 were 13.3% and 28%, respectively.

Figure 6 indicated that the activity of WO_3/webnet catalyst declined significantly after 4 h reaction and the photocatalytic conversion of primary reactants reached to approximately stable amounts. It seems that the stability in the conversion of CH_4 and CO_2 can be due to adsorption of gaseous reactants and accumulation of products on the photocatalyst surface. Similar results have been reported on the performance of other semiconductor photocatalysts[3,7,10,11]. It may be say that with passing time of the reaction, the products accumulate on the catalyst surface and it has two inefficient effects, backward reactions and deactivation of active sites that consequently cause the saturation of conversion rate[10]. Also, the reported results demonstrated that photocatalysts are deactivated by accumulation of surface species formed during the reaction. The characterization of intermediate products has been verified that intermediate products that are retained on the surface can lead to a number of problems include catalyst deactivation[47]. Liu *et al.* reported that the intermediates such as acetic acid and formic acid were produced in the degradation process and the desorption rate of acetate and formate from TiO_2/WO_3 composite photocatalyst was considerably lower than the rate for their catalytic oxidation. This product accumulation on photocatalyst surface declines reaction rate slowly. The above phenomenon also suggested that these intermediates occupied the active sites on catalyst surface resulting in the decrease of the degradation activity[48]. Also, for comparison purposes, photodegradations of CH_4 and CO_2 over TiO_2/webnet and ZnO/webnet catalysts were measured under identical experimental conditions. The photo-conversion of CH_4 and CO_2 was not observed with the TiO_2/webnet and ZnO/webnet catalysts under visible irradiation, since TiO_2 and ZnO could not be excited by the illumination of visible light. So, the photocatalytic activity of WO_3/webnet catalyst was better than those of TiO_2/webnet and ZnO/webnet.

As both of CO_2 and CH_4 are carbon containing compounds, the formation of heavier products with more than one carbon atom would be expected. Figure 7 represents a possible reaction mechanism for photocatalysis of CO_2 + CH_4[4,7,10-11,13,15,49-51]. It must be noted that C_2H_4 can also be generated by oxidation of CH_3CH_3 via valence band holes to $\cdot CH_2CH_3$ which gives CH_2CH_2 and $\cdot H$ through an elimination reaction activated by photons. Moreover, C_2H_2 production is possible through $CO \rightarrow \cdot CO^- \rightarrow \cdot C \rightarrow \cdot CH_2 + \cdot H \rightarrow C_2H_2$ route[49].

Also, It is important to study the reactivity of a photocatalyst during photocatalysis process. We tried

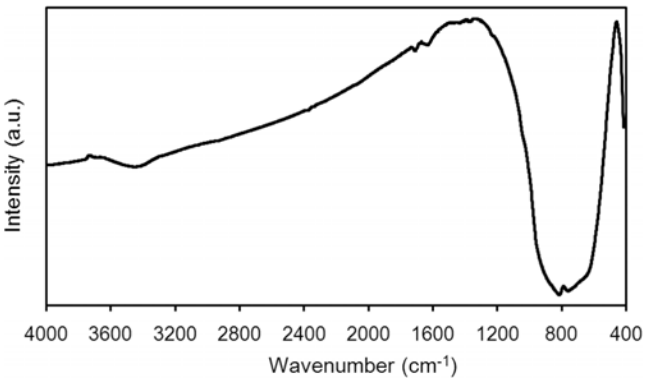

Fig. 4 — FTIR spectra of the synthesized WO_3 nanoparticles.

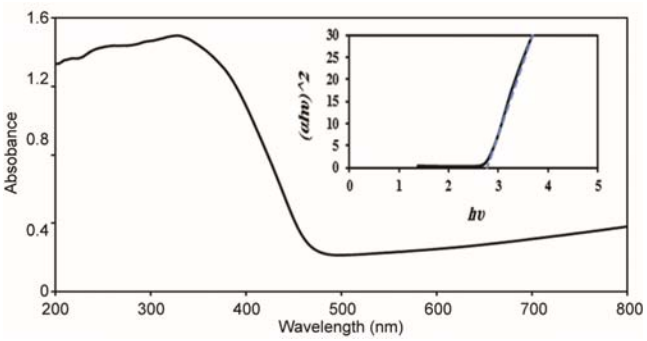

Fig. 5 — (a) UV-vis spectra of synthesized WO_3 nanoparticles (b) Inset shows the Tauc plot of synthesized WO_3 nanoparticles for the purpose of band gap calculation.

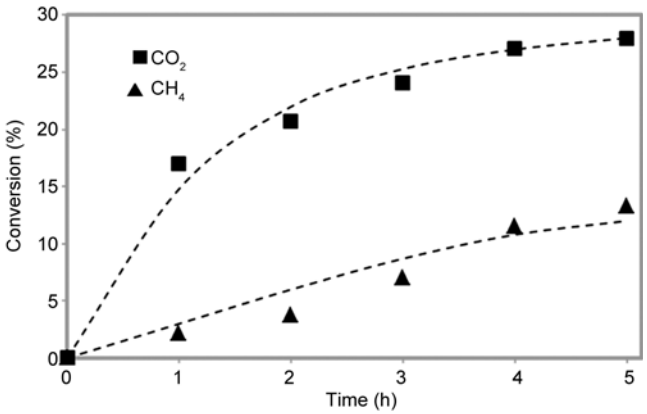

Fig. 6 — The photocatalytic conversions of CO_2 and CH_4 over WO_3/120 mesh webnet catalyst (feed composition: 45% CO_2:45%CH_4:10%He).

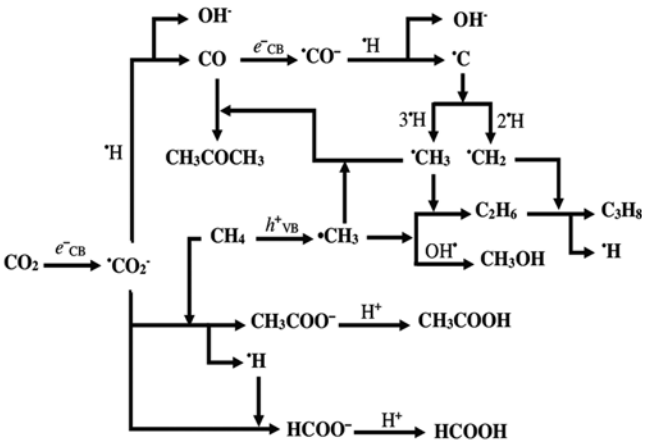

Fig. 7 — The proposed reaction mechanism of photocatalysis of $CO_2 + CH_4$[49].

to regenerate the efficient photocatalyst (WO_3) for two times by heat treatment of the deactivated photocatalyst at 300°C to desorb the adsorbed species. The reusability analyses of WO_3 for three runs shows that the photocatalytic activity of 26.32 and 22.12% were provided after each regeneration. The photocatalytic efficiency of WO_3 is comparable with other gas phase photocatalysts. For example, in our previous reports on CO_2 reduction at the same conditions, the fresh photocatalysts of CuPc/TiO_2 showed only 14% CO_2 conversion after 4 h and under visible light irradiation[10].

Conclusion

In this study, the direct photocatalytic conversion of CO_2 and CH_4 concurrently in gas-phase batch reactor under visible light irradiation by WO_3 nanoparticles coated on stainless steel webnet has been investigated. Monoclinic WO_3 nanoparticles were successfully synthesized by a simple and inexpensive method. The band gap energy of the m-WO_3 nanoparticles was 2.77eV, indicating good visible light harvesting ability. Compared to the commercial TiO_2 and ZnO, the synthesized m-WO_3 nanoparticles exhibit a superior photocatalytic activity for conversion of CO_2 and CH_4 under visible light irradiation. The maximum percentage conversions of 28% for CO_2 and 13.3% for CH_4 were observed by WO_3/visiblie light. However, the conversions of CO_2 and CH_4 under unmodified TiO_2 and ZnO and visible light were zero.

References

1 Koci K, Obalova L & Lacny Z, *Chem Pap*, 62 (2008) 1.
2 Centi G, Perathoner S & Rak Z S, *Appl Catal B: Environ*, 41 (2003) 143.
3 Merajin M T, Sharifnia S & Mansouri A M, *J Taiwan Inst Chem Eng*, 45 (2014) 869.
4 Yuliati L, Itoh H & Yoshida H, *Chem Phys Lett*, 452 (2008) 178.
5 Kamat P V, *Chem Rev*, 93 (1993) 267.
6 Hagfeldt A & Graetzel M, *Chem Rev*, 95 (1995) 49.
7 Shi D, Feng Y & Zhong S, *Catal Today*, 98 (2004) 505.
8 Kohno Y, Tanaka T, Funabiki T & Yoshida S, *Phys Chem Chem Phys*, 2 (2000) 5302.
9 Teramura K, Tanaka T, Ishikawa H, Kohno Y & Funabiki T, *J Phys Chem B*, 108 (2004) 346.
10 Yazdanpour N & Sharifnia S, *Sol Energy Mater Sol Cells*, 118 (2013) 1.
11 Merajin M T, Sharifnia S, Hosseini S N & Yazdanpour N, *J Taiwan Inst Chem Eng*, 44 (2013) 239.
12 Mahmodi G, Sharifnia S, Rahimpour F & Hosseini S N, *Sol Energy Mater Sol Cells*, 111 (2013) 31.
13 Mahmodi G, Sharifnia S, Madani M & Vatanpour V, *Sol Energy*, 97 (2013) 186.
14 Delavari S & Amin N A S, *Appl Energy*, 162 (2016) 1171.
15 Delavari S, Amin N A S & Ghaedi M, *J Clean Prod*, 111 (2016) 143.
16 Arai T, Yanagida M, Konishi Y, Ikura A, Iwasaki Y, Sugihara H & Sayama K, *Appl Catal B: Environ*, 84 (2008) 42.
17 Bi Y, Ehsan M F, Huang Y, Jin J & He T, *J CO_2 Util*, 12 (2015) 43.
18 Bai S, Zhang K, Sun J, Luo R, Li D & Chen A, *Cryst Eng Comm*, 16 (2014) 3289.
19 Takeuchi M, Shimizu Y, Yamagawa H, Nakamuro T & Anpo M, *Appl Catal B: Environ*, 110 (2011) 1.
20 Sayama K, Hayashi H, Arai T, Yanagida M, Gunji T & Sugihara H, *Appl Catal B: Environ*, 94 (2010) 150.
21 Zheng Q & Lee C, *Electrochimica Acta*, 115 (2014) 140.
22 Chen X, Zhou Y, Liu Q, Li Z, Liu J & Zou Z, *ACS Appl Mater Interface*, 4 (2012) 3372.
23 Wang P Q, Bai Y, Luo P Y & Liu J Y, *Catal Commun*, 38 (2013) 82.
24 Ohno T, Murakami N, Koyanagi T & Yang Y, *J CO_2 Util*, 6 (2014) 17.
25 Noceti R P, Taylor C E & D'Este J R, *Catal Today*, 33 (1997) 199.
26 Taylor C E & Noceti R P, *Catal Today*, 55 (2000) 259.
27 Taylor C E, *Catal Today*, 84 (2003) 9.
28 Gondal M A, Hameed A & Suwaiyan A, *Appl Catal A: General*, 243 (2003) 165.
29 Gondal M A, Hameed A, Yamani Z H & Arfaj A, *Chem Phys Lett*, 392 (2004) 372.
30 Hameed A, Ismail I M I, Aslam M, Gondal M A & Gondal, *Appl Catal A: General*, 470 (2014) 327.
31 Villa K, Murcia-Lopez S, Andreu T & Morante J R, *Catal Commun*, 58 (2015) 200.
32 Villa K, Murcia-Lopez S, Andreu T & Morante J R, *Appl Catal B: Environ*, 163 (2015) 150.
33 Boudiba A, Roussel P, Zhang C, Olivier M G, Snyders R & Debliquy M, *Sens Actuators B*, 187 (2013) 84.
34 Boudiba A, Zhang C, Navio C, Bittencourt C, Snyders R & Debliquy M, *Procedia Eng*, 5 (2010) 180.
35 Hosseini S N, Borghei S M, Vossoughi M & Taghavinia N, *Appl Catal B*, 74 (2007) 53.
36 Qin S, Xin F, Liu Y, Yin X & Ma W, *J Colloid Interface Sci*, 356 (2011) 257.
37 Zhang Q H, Han W D, Hong Y J & Yu J G,*Catal Today*, 148 (2009) 335.

38 Taheri Najafabadi A & Taghipour F, *J Photochem Photobiol A*, 248 (2012) 1.
39 Tseng H, Wu G C S & Chou H Y, *J Catal*, 221 (2004) 432.
40 Xu F, Yao Y, Bai D, Xu R, Mei J, Wu D, Gao Z & Jiang K, *RSC Adv*, 5 (2015) 60339.
41 Adhikari S, Sarkar D & Maiti H S, *Mater Res Bull*, 49 (2014) 325.
42 Daniel M F, Desbat B, Lassegues J C, Gerand B & Figlarz M, *J Solid State Chem*, 67 (1987) 235.
43 Ho G W, Chua K J & Siow D R, *Chem Eng J*, 181 (2012) 661.
44 Rashad M M & Shalan A E, *Appl Phys A*, 116 (2014) 781.
45 Xin G, Guo W & Ma T, *Appl Surf Sci*, 256 (2009) 165.
46 Zhang H, Yang J, Li D, Guo W, Qin Q, Zhu L & Zheng W, *Appl Surf Sci*, 305 (2014) 274.
47 Mendez-Roman R & Cardona-Martinez N, *Catal Today*, 40 (1998) 353.
48 Liu Y, Xie C, Li H, Chen H, Liao Y & Zeng D, *Appl Catal B: Environ*, 102 (2011) 157.
49 Karamian E & Sharifnia S, *J CO_2 Util*, 16 (2016) 194.
50 Tahir M, Tahir B & Saidina Amin N, *Mater Res Bull*, 63 (2015) 13.
51 Yarahmadi A & Sharifnia S, *Dyes Pigm*, 107 (2014) 140.